Published in
Quantum Sensing and Nanophotonic Devices VII (Proceedings of SPIE) 7608, issue 76081N, 1-11, 2010
which should be used for any reference to this work

Mid-infrared quantum cascade detectors for applications in spectroscopy and pyrometry

Daniel Hofstetter
University of Neuchatel, Avenue de Bellevaux 51, CH – 2009 Neuchatel, Switzerland

Fabrizio R. Giorgetta, Esther Baumann
Optoelectronics division, National Institute of Standards and Technology, 325 Broadway, Boulder, CO 80305, USA

Quankui Yang, Christian Manz, Klaus Köhler
Fraunhofer Institute for Applied Solid State Physics, Tullastrasse 72, D – 79108 Freiburg i. Brsg., Germany

ABSTRACT

An overview of quantum cascade detector technology for the near- and mid-infrared wavelength range will be given. Thanks to photovoltaic instead of photoconductive operation, quantum cascade detectors offer great opportunities in terms of detection speed, room temperature operation, and detectivity. Besides some crucial issues dealing with fabrication and general characteristics, some possibilities for performance improvement will also be briefly presented. In a theory section, some basic considerations adopted from photoconductive detectors confirm the necessity of various trade-offs for the optimization of such devices. Nevertheless, we will show several possible measures to push the key performance figures of these detectors closer to their physical and technological limits.

Keywords: Intersubband photodetectors, quantum cascade detector, high-speed semiconductor photodetectors.

1. INTRODUCTION

Intersubband (ISB) photodetectors have become key components for many applications in the mid-infrared wavelength range. Although their first demonstration lies already more than twenty years back, they remain a topic of high scientific interest. Early demonstrators were based on photoconductive effects; and due to the importance of the quantum well (QW)-based active region, Levine et al. called these devices quantum well infrared photodetectors (QWIPs) (1). It was soon discovered that such QWIPs have many unique properties, especially regarding high frequency operation. In an interband device, the parasitic capacitance of the p-n-junction will always be the limiting factor. However, since ISB detectors are unipolar, their fundamental speed limit is the ISB scattering time which is determined by a highly efficient electron-phonon scattering process with typical lifetimes of $\tau_{scatter} \approx 1$ ps. For QWIPs, this results typically in cutoff frequencies on the order of 100 GHz (2). As a further advantage, ISB detectors can be designed for a wide range of wavelengths using a single material system. This is achieved by choosing adequate semiconductor layer thicknesses. This is in sharp contrast to interband devices, where the bandgap determines to a large extent the detectable photon energy.

A very complete introduction on the working principles of ISB infrared photodetectors is presented in a book by H.C. Liu and H. Schneider (3). Starting with a simple classification, one can distinguish between photoconductive and photovoltaic detectors. In the class of photoconductive devices, the most common detector is the QWIP, where the change of device resistance under illumination is measured. There are various types of QWIPs; they differ mainly by the kind of ISB transition exploited. According to the position of the upper quantized detector level, the optical transition can be either bound-to-quasi-bound (4) or bound-to-miniband (5). In the widely used bound-to-quasi-bound QWIP, which was also the first ISB detector to be demonstrated in 1987, the detection energy depends on the conduction band discontinuity between the quantum well (QW) and the barrier material. The QW thickness and conduction band discontinuity (through the material composition) are chosen such that the second quantized electronic level is almost in

resonance with the barrier's conduction band edge; this measure ensures a good carrier extraction efficiency under application of an appropriate bias voltage. By using the bound-to-miniband design, the QWIP detection wavelength will be decoupled from the conduction band discontinuity. Nevertheless, a quite precise resonance condition between the upper detector state and the miniband states must be fulfilled in order to obtain a good responsivity. Nowadays, state-of-the-art QWIP-based focal plane arrays sensitive at wavelengths between 8 µm and 10 µm have reached commercial maturity. As a particularly advanced example of such an infrared camera, Gunapala et al. presented a high performance 1024 x 1024 pixel dual band focal plane array based on GaAs / AlGaAs with cutoff wavelengths of 5.1 µm and 8.4 µm (6). Major advantages of such photoconductive ISB detectors are a competitive responsivity and a good detectivity, especially at low operating temperatures. However, the quite considerable dark current of QWIPs leads to a non-negligible noise which dominates the detectivity at higher temperatures. Unfortunately, this drawback is not entirely compensated by the high responsivity. In contrast, a photovoltaic ISB detector profits from the fact that there is no dark current and thus no dark current noise. But since such a device has no photoconductive gain and therefore a lower responsivity, the better noise behavior can at least partly make up for these shortcomings.

Considering all these facts, it is astonishing that over the years, the development of photovoltaic ISB photodetectors has attracted less interest. Already back in 1991, Schneider et al. (7), (8) observed pronounced photovoltaic effects in an asymmetric multi QW structure. The potential asymmetry was obtained via a sheet of delta-doping close to the active QW. As shown by Schneider as well, optimized photovoltaic QWIPs have superior noise properties, the capability to operate at higher photon fluxes, and an improved dynamical range in comparison to a photoconductive QWIP (9). Especially with respect to the improved noise behavior, it is thus no surprise that the first QW-based infrared detector for THz radiation was a photovoltaic device rather than a photoconductive QWIP (10), (11). A similar ISB detector for mid-infrared wavelengths was later presented by Gendron et al. (12); in analogy to the functioning of a quantum cascade laser (QCL), this device was named quantum cascade detector (QCD). In such a QCD, the asymmetric potential used for unilateral carrier transport is formed by a series of QWs with increasing thicknesses. Interesting enough, a QCD-like semiconductor structure was invented already in 1987 under the name ‘optical charge pump’ (13). Like the bound-to-miniband QWIP, this device offers more design freedom for a given material composition. A very schematic comparison between the band structures of a photoconductive QWIP and a photovoltaic QCD is shown in figure 1.

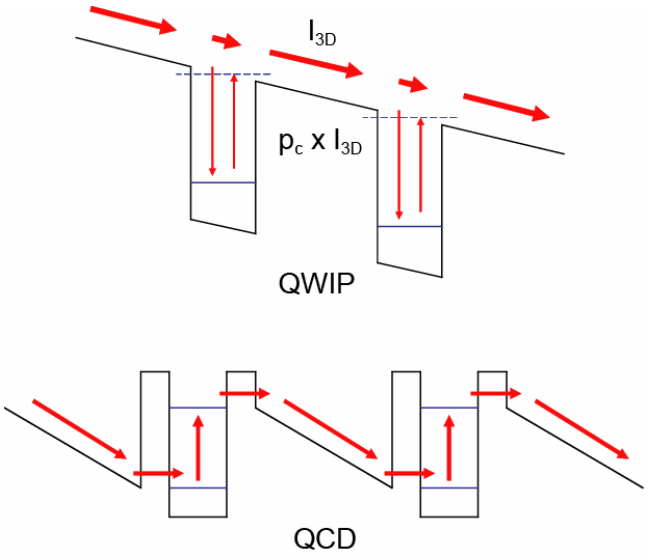

Fig. 1 - Schematic conduction band diagram of a QWIP and a QCD. In the QWIP, electron transport is accomplished by an external voltage bias whereas in a QCD, an internal potential ramp ensures the carrier transport.

Compared to a QWIP, the absence of dark current noise is not the only advantage of a QCD. The missing dark current also prevents capacitance saturation in the read-out circuit and thus allows longer integration times. Finally, the thermal load of the detector is strongly reduced, which is of interest if the available cooling is limited, for example in space-born or hand-held terrestrial staring systems. As a final point, the somewhat narrower linewidth of QCDs compared to QWIPs results in a reduced background photon noise. Although QCDs have already progressed a lot (14), they do not yet take

full advantage of their potentially low Johnson noise; mainly because of an insufficiently high room temperature device resistance. Our most recent results, which will be presented in this paper, show nevertheless that QCDs with competitive performance can be achieved using improved designs.

We will discuss the design principles of QCDs as well as the choice of material system for the different detection wavelengths. Experimental results of QCDs at various wavelengths are reviewed. First, QCDs based on InGaAs / InAlAs lattice matched to InP detecting between 4.7 μm and 10 μm are presented. As lattice matched InGaAs QCDs can only detect wavelengths above ~ 4 μm due to the conduction band discontinuity of 520 meV, an alternative approach is presented for shorter wavelengths: lattice-matched InGaAs / AlAsSb. Finally, a broadband QCD covering the wavelength region from 4.7 to 7.4 μm is shown. We will also discuss some of the trade-offs to be made when designing improved QCDs; they will lead to certain guidelines for detectors with particular applications.

2. BASIC QCD THEORY

Following the terminology of M.A. Reed et al. in 1987, one can understand the QCD as an optical charge pump. The 'engine' driving this pump is the incoming flux of photons, the pumped charges are the electrons, and the entire device is unidirectional because of its saw-tooth shaped potential. Each electron has first to be lifted on the steep side and then slides down the sloped side of a tooth. The electro-optical behavior of QCDs can be described using exactly the same theory as in QWIPs. The basic optical process for mid-infrared detectors such as QWIPs or QCDs is the ISB transition (15). In contrast to interband transitions, ISB transitions result in relatively narrow and peaked absorption features, whereas interband transitions are characterized by spectrally large absorption features with a cut-off wavelength. The main reason for this striking difference is the opposite curvature of the electron and hole dispersion curves in the interband case and the parallel curvature of the electronic subbands in the ISB case. The current responsivity of a QCD, R_p, is defined as detector output current I_S per unit of input signal power P_S and is given by

$$R_p = \frac{I_S}{P_S} = \frac{q}{h\upsilon}\eta g_p = \frac{\lambda q}{hc}\eta g_p;\ \ g_p = \frac{p_e}{N_{QW}p_c} \qquad (1)$$

where $\nu = c/\lambda$ is the signal frequency, λ the signal wavelength, c the vacuum speed of light, q the elementary charge, h Planck's constant, η the absorption efficiency, and g_p the photodetector (photoconductive) gain. Furthermore, p_e is the escape probability of an excited electron in the active QW, p_c its capture probability into the active QW ground state, and N_{QW} the number of active QWs. Optimization of R is thus accomplished through improvement of both absorption efficiency and photodetector gain. For sufficiently low absorptions, the total absorption efficiency is proportional to the absorption efficiency of a single QW. However, since the detector gain is inversely proportional to the number of QWs, the current responsivity is in first approximation independent from the number of periods.

An important figure of merit for photodetectors is their detectivity $D^* = R_p / i_n\sqrt{A\Delta f}$, which is the ratio between peak responsivity R_p and mean noise current i_n (or the inverse noise equivalent power) properly normalized by the detector area A and the measurement bandwidth Δf. Its units are cm $Hz^{0.5}$/W, also known as Jones. For any given infrared detector, the detectivity D^* reveals two distinct temperature regimes. At low temperatures, D^* is dominated by photon noise due to the 300 K blackbody radiation seen by the device. This is the background limited operating (BLIP) regime. Above a certain temperature, T_{BLIP}, other noise mechanisms become dominant. As we have stated above, a QWIP's detectivity, D^*, at $T > T_{BLIP}$ is determined by dark current noise, whereas the one of a QCD is dominated by Johnson noise. Taking into account these different facts, we get for the detectivity of a QCD

$$D_J^* = R_p\sqrt{\frac{R_0 A}{4k_B T}}$$

$$D_{BLIP}^* = \frac{R_p}{\sqrt{2q^2 g_p \int g_p \eta(\nu')\frac{d\Phi_{BG}(\nu')}{d\nu'}d\nu'}} \qquad (2)$$

where R_0 is the differential device resistance around 0 V, T the device temperature, and $d\Phi_{BG}(\nu')/d\nu'$ the spectral background photon flux density. For a QCD, D^* is maximized by ensuring a high device resistance (thus a low Johnson noise) without lowering the escape probability and thus the detector gain. At the same time, one should try to optimize the absorption efficiency without decreasing the device resistance. This can be done via doping optimization or external measures such as surface grating couplers, waveguides, or lenses. The most important 'internal' design parameters are the layer thicknesses (determining the band profile as discussed below), the doping density n_s of the active QW, and the number of periods N_{QW}.

3. EXPERIMENTAL QCD DESIGN

The quantum-mechanical polarization selection rule (16) dictates that only the electric field component perpendicular to the QW layers interacts with ISB transitions. Therefore, vertical incidence of the incoming radiation has to be avoided. Possible device geometries taking into account the polarization selection rule include a 45° wedge multi-pass geometry, the Brewster geometry, or a surface grating. The particular choice of sample preparation is determined by factors such as the absorption strength of the sample or the specific application case of the detector.

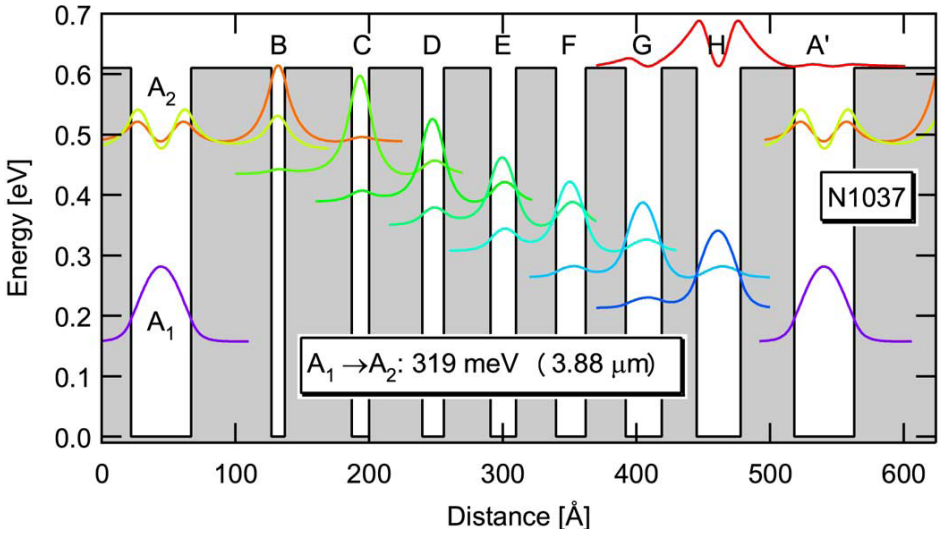

Fig. 2 - Calculated conduction band profile of a QCD for 3.9 μm. QW A is the active QW, QWs B to H form the extractor cascade.

The most crucial design aspect of ISB devices is the quantum mechanical bandstructure. It can be calculated using numerical Schrödinger equation solvers. A typical band structure of a QCD is shown in figure 2. QW A is the active doped QW, while QWs B-H form the nominally undoped electron extraction cascade. The asymmetry of the bandstructure, as we have seen it already in figure 1, is clearly visible. The transport from the active QW into the extraction region is guaranteed via a resonant tunneling process between A_2 and the ground state of the much narrower QW B; this allows for a thick barrier between the active QW and the extractor. To achieve an efficient electron extraction through phonon assisted scattering, the energy difference between the individual extractor states should be close to the longitudinal optical phonon energy E_{LO} (GaAs: E_{LO} = 36 meV, $In_{0.53}Ga_{0.47}As$: E_{LO} = 32 meV). More recently, we have made successful tests using smaller energy separations between extractor states. By doing so, one can increase the total barrier thickness and thus the room temperature device resistance. The resulting influence on the detection speed has yet to be determined. In such a modified extraction cascade, transport is accomplished mainly via interface roughness scattering.

4. EXAMPLES OF QCD DEVICES

There are various photodetector applications in the mid-infrared spectral range. They include pyrometry, spectroscopy, night vision, and sensing of hot spots. In the first part of this section, experimental results obtained from

QCDs sensitive at wavelengths between 4.7 µm and 10 µm (136 meV – 268 meV) are presented. The investigated samples consist of $In_{0.52}Ga_{0.48}As$ QWs and $In_{0.53}Al_{0.47}As$ barriers lattice matched to InP substrates. All layer structures were grown by molecular beam epitaxy (MBE) in order to achieve a high interface quality between QWs and barriers. During MBE growth, a valved cracker cell for the As and effusion cells for In, Al, Ga and Si were used. Reflection high energy electron diffraction (RHEED) allowed a continuous monitoring of the layer morphology. Growth started with a 6000 Å thick $In_{0.53}Ga_{0.52}As$ lower contact layer followed by 30 repetitions of the active region and a 2000 Å thick $In_{0.53}Ga_{0.47}As$ upper contact layer. Details on the layer thicknesses can be found in reference (17). X-ray diffraction measurements and visual inspection using an optical microscope allowed us to assess the crystal quality after growth. From a design point of view, the samples shown here are based on the QCDs presented in reference (18). As mentionmed above, they have already somewhat thicker barriers to increase device resistance. After growth, the samples were polished into 45º multi-pass waveguides for absorption tests. For photocurrent measurements, mesas were processed using standard photolithography and wet etching. Contacting was obtained through evaporated metal contacts. Device testing was done in a liquid-He flow cryostat under temperatures ranging from 10 K up to room temperature, while illumination was accomplished via the internal globar light source of the spectrometer. The detector signals were amplified using a Stanford research SR570 current amplifier whose output signal was fed back into the Fourier spectrometer.

4.1 Mid-infrared QCDs

In the following paragraph, we present three examples of mid-IR QCDs. All of them are designed for specific laser wavelengths, namely 4.7 µm, 7.5 µm, and 10.0 µm. Although they span a considerable wavelength range, their performances turned out quite comparable. The same number of active region periods (30) was used for the three samples. The doping levels of the main QW were adapted to result in responsivities of roughly 10 mA/W.

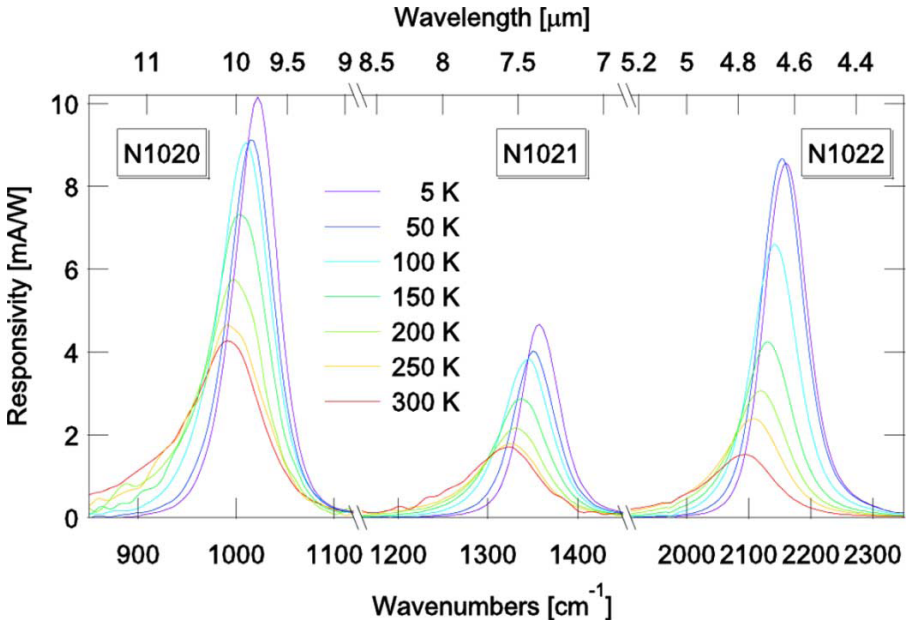

Fig. 3 - Responsivity of the ISB A1 → A2 transition of a 10 µm device (left), a 7.5 µm device (center), and a 4.7 µm QCD (right) at different temperatures.

Fig. 3 shows the measured responsivity spectra of the samples for temperatures between 5 K and 300 K. For the two shorter wavelength samples, the peak detection energies of 268 meV and 168 meV correspond well to the simulated ones of 266 meV and 165 meV, respectively. For the longer wavelength sample, the observed value of 127 meV is slightly too large with respect to the designed 118 meV. In the latter case, the somewhat larger difference between designed and experimental transition energy can be explained by a slightly too small superlattice period. The observed redshift of detection energy with increasing temperature (127 meV at 5 K, 123 meV at 300 K) is typical for QCDs and caused by band filling and non-parabolicity of the electron states (19).

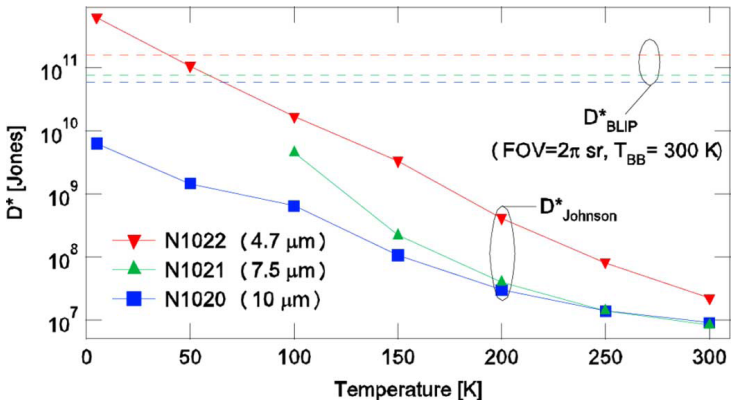

Fig. 4 - Detectivities D^* of the three QCDs (4.7 µm: downward triangles, 7.5 µm: upward triangles, 10 µm: squares) shown in the previous figure as a function of temperature. D^* is Johnson noise limited except for the 4.7 µm QCD below T_{BLIP} = 45 K. The dashed lines on top represent the background limited detectivity D^*_{BLIP} for a hemispherical field of view and a background temperature of 300 K.

Fig. 4 shows the Johnson noise limited detectivity for all three samples as a function of temperature obtained with equation (2) and using measured values for both the responsivity and the resistance-area product R_0A; the constant background limited detectivities are also shown as dashed horizontal lines. The detectivity of the 4.7 µm QCD (downward triangles) becomes background limited at T_{BLIP} = 45 K and is on the order of 2 x 10^{11} Jones. Because of a too low device resistance, the two other QCDs (7.5 µm: upward triangles, 10 µm: squares) show detectivities remaining below D^*_{BLIP} for all investigated temperatures. Besides too thin barriers, an intrinsic effect is responsible for the lower detectivities. Due to the small transition energy of these long wavelength devices, electron can couple to the ground states of adjacent QWs. We were able to verify this hypothesis by Arrhenius plots of the differential resistance around 0 V. They reveal an activation energy which is roughly 70 % of the optical transition energy. This undesired effect can be reduced by pushing the extractor states to a higher energetic level, and has been experimentally verified in the broadband QCD described below.

4.2 Antimony-based near-IR QCD

To obtain ISB detectors working at wavelengths below 3 µm, the QCD design was also successfully applied to the $In_{0.53}Ga_{0.44}As$ / $AlAs_{0.56}Sb_{0.44}$ material system lattice matched to InP substrates. This material system offers a conduction band discontinuity of 1.6 eV. Other advantages are that the mature processing technology of the InGaAs / InAlAs system can be used, that growth of the InGaAs QWs is well established, and that high quality InP substrates are available at reasonable cost. The difficulties lie in the growth of the $AlAs_{0.56}Sb_{0.44}$ barrier material and the barrier / QW interface quality. In real devices, the resulting interface fluctuation between QWs and barriers is a limiting factor towards high ISBT energies [20].

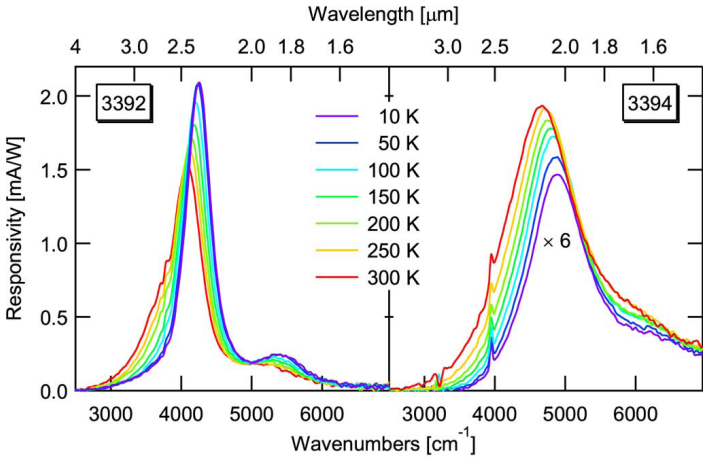

Fig. 5 - Responsivity spectra of AlAsSb QCDs for different temperatures. Left panel: 3392 detecting around 4065 cm^{-1} (2.45 μm). The shoulder at 1.82 μm is due to the diagonal transition from the active QW's ground state into the last extractor QW's excited state. Right panel: responsivity of 3394 detecting around 2.05 μm scaled by a factor of 6.

In Fig. 5, the responsivity spectra of samples 3392 and 3394 are depicted [21]. The responsivity peaks at 605 meV (2.05 μm) for 3394 and at 528 meV (2.35 μm) for 3392. Interface roughness is responsible for both large relative linewidths on the order of 10 % for 3392 and even 20 % for 3394; and for a roughly 15 % longer detection wavelength as compared to the simulations. Especially problematic in this context is the small QW thickness along with a considerable interface roughness. Together, this results in a kind of intermixed QW with a 'round' instead of a square-shaped bottom. The ground state of such a QW is then pushed up and leads to smaller transition energies than expected. The Johnson noise limited detectivities D^* of 3392 and 3394 were calculated using measured values for the peak responsivity R_p and the resistance-area product R_0A. At 300 K, 3392 has a detectivity of D^* of 8.2 x 10^7 Jones; the corresponding value for 3394 is D^* = 1.2 x 10^7 Jones. D^*_{BLIP} amounts to 1.15 x 10^{12} Jones and 1.47 x 10^{11} Jones for 3392 and 3394, respectively. In a later attempt (EP745), a better performance of the 2.45 μm QCD could be achieved by the use of AlAs interdiffusion layers and thicker barriers. Its responsivity is shown in figure 6. Compared to 3392, two main differences are observed: the linewidth of EP745 is 35 % smaller and the high energy shoulder at 5400 cm^{-1} is no longer present. The thicker barrier layers resulted also in a much higher device resistance. As a consequence of the elevated resistance-area product, EP745's Johnson noise was low and the Johnson noise limited detectivity D^* was high, namely 2.9 x 10^{10} Jones at 200 K. If the calculated D^* are extrapolated towards lower temperatures, D^* equals the 300 K background limited hemispherical D^*_{BLIP} = 1.15 x 10^{12} Jones at T_{BLIP} = 100 K.

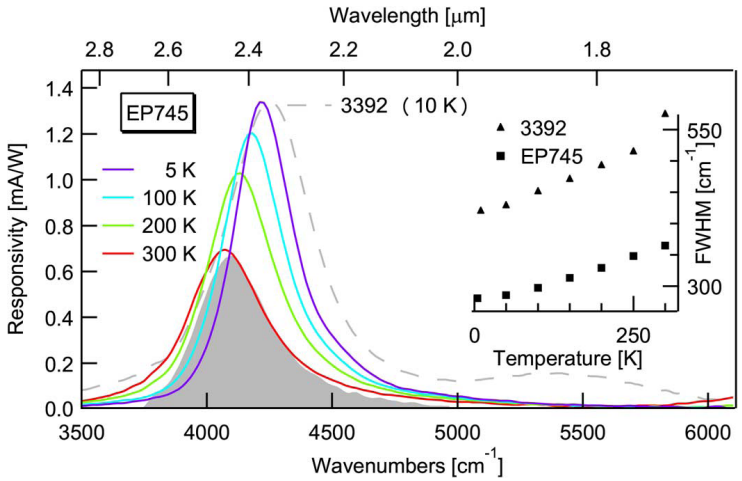

Fig. 6 - Responsivity of AlAsSb QCD EP745 at different temperatures (solid lines). The dashed line is the responsivity of III-3392 at 10 K scaled by a factor 0.64. The shaded area is the room temperature absorption per double pass of EP745 with a peak value of 3.4%. The inset compares the FWHM of EP745 to an earlier sample 3392.

Another benefit of the thicker extractor barriers is the higher oscillator strength and thus absorption efficiency of the main optical transitions. The overall extraction efficiency did not suffer from a thicker barrier at the low-energy end of the extractor: once an extracted electron reaches the thicker barrier, its recapture probability into the active QW from where it originated is negligible. The fabrication of these short-wavelength QCDs has shown that 2.0 µm can be regarded as the lower wavelength limit of antimony-based devices. Although a good detectivity could be reached, such detectors are unfortunately not yet really competitive on the market.

4.3 Spectrally broad QCD

Up to late 2008, it was not clear whether a QCD with a spectrally broad response on the order of roughly $\Delta\nu/\nu$ = 25 % would have comparable noise properties as a standard narrow response ($\Delta\nu/\nu$ = 5 %) QCD. Recently, a mid-infrared QCD based on lattice matched InGaAs / InAlAs with a relative linewidth of 27 % was designed and fabricated by Hofstetter et al. (22). It makes use of 26 carefully designed active region stages – the term 'period' is no longer appropriate in this device - spanning a wavelength range between 4.6 and 7.4 µm (10 % values of the responsivity).

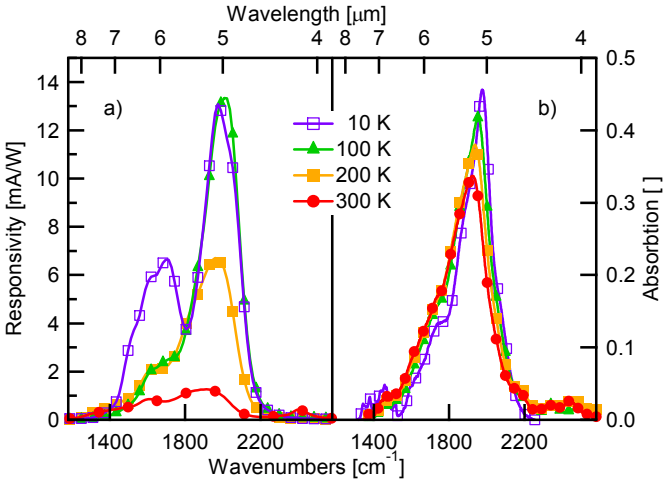

Fig. 7 - Responsivity (a) and absorption (b) spectra of the broadband QCD at 10 K, 100 K, 200 K, and 300 K.

As shown in figure 7(a), the 10 K responsivity peaks at 1950 cm^{-1} (E = 242 meV) with 13 mA/W. The FWHM at this low temperature is 420 cm^{-1} (ΔE = 52 meV, ΔE/E = 21.5 %). When going to room temperature, a responsivity of 1.25 mA/W peaking at 1920 cm^{-1} (E = 238 meV) was observed, with a FWHM of 525 cm^{-1} (ΔE = 65 meV, ΔE/E = 27.3 %). Absorption spectra measured using a multi-pass zigzag waveguide configuration are shown in figure 7(b) for selected temperatures of 10, 100, 200, and 300 K. They show the usual slight broadening and low energy shift with temperature; and they agree quite well with the responsivity curves at the corresponding temperatures.

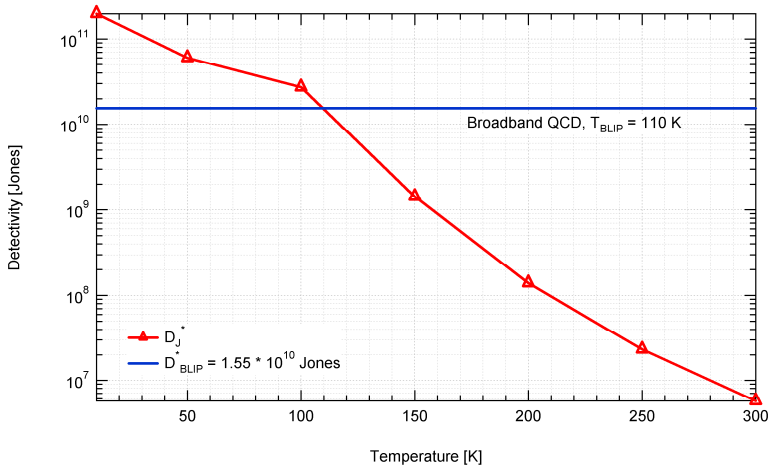

Fig. 8 - Detectivity of the broadband QCD as a function of temperature along with a calculated value of the background limited detectivity.

Despite of the large detection spectrum, the noise properties of this device were not too adversely affected: as presented in figure 8, the background limited detectivity amounts to 1.55×10^{10} Jones up to a temperature T_{BLIP} of 110 K. Although performance-wise not yet being fully optimized, this device is a first step towards semiconductor based ISB detectors for spectrally broad applications such as spectroscopy.

5. OUTLOOK

As figure 9 shows, it is quite obvious that the detectivities of the shorter mid-infrared devices are closest to the theoretical maximum. Therefore, any future effort will concentrate on an improvement of the detectivity of QCDs in the technologically most important 5 – 10 µm or mid-infrared wavelength range. We further notice that for each specific application of a QCD, a different set of parameters needs to be optimized. For a detector in pyrometry, the reponsivity close to room temperature should be as large as possible, while spectrally narrow detection is not necessarily an advantage. In highly sensitive spectroscopy applications, a narrow detection window together with a good detectivity would be highly desirable. For applications such as heterodyne spectroscopy, high frequency operation would be required. In a night vision system, finally, one would like to profit from a good detectivity, but not necessarily at room temperature. Such a system could very well function at cryogenic temperatures and at low frequencies. Several of the requirements of such a hypothetical wish list are contradictory; therefore, one has to make trade-offs. For instance, someone could be tempted to increase the room temperature resistance by making very thick barrier layers. This would result in a better Johnson noise behavior, but since thick barriers will decrease the tunneling probabilities, the detector would certainly end up slower than before. Additional measures to improve the responsivity include the use of immersion lenses and more sophisticated surface structures to efficiently capture the incoming radiation.

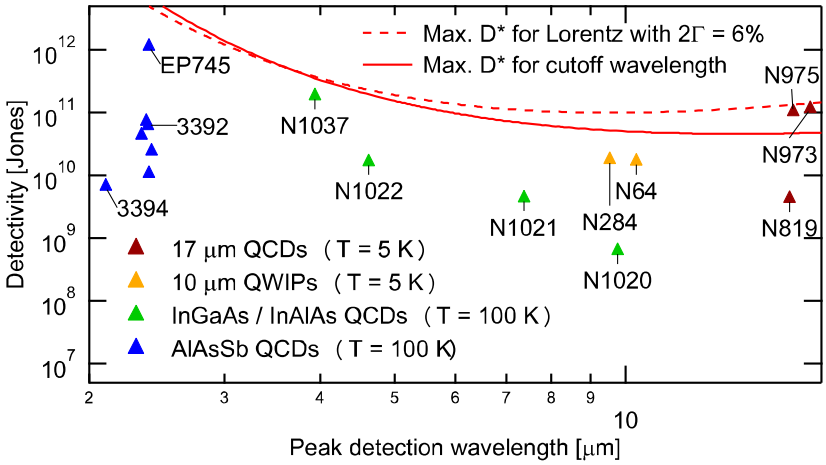

Fig. 9 - Detectivity as a function of detection wavelength for all near- and mid-infrared QCDs presented in this article. It is obvious that the devices between 7 and 10 μm offer a considerable potential for improvement.

For highest speed operation, it is clear that phonon resonance and efficient scattering processes in the extraction region are an absolute necessity. For this reason, barrier layer thicknesses should not be too large. As the recently demonstrated 23 GHz cutoff frequency of a QCD has shown, a more sophisticated sample mounting adapted to high frequency operation will have a positive effect on the detector speed. Together, these measures should enable detector operating frequencies closer to the theoretical maximum.

6. CONCLUSIONS

QCDs are a promising technology which works well at wavelengths between near infrared and far-infrared wavelengths. Similar as in QC lasers, the theoretical prediction of QCD wavelengths is very reliable. Especially in the mid infrared range around 4 to 17 μm, well-known semiconductor material systems and processing methods are available. In this article, QCDs in the near-IR fabricated from InGaAs/AlAsSb and in the mid-IR using InGaAs/InAlAs materials were presented. THz QCDs have already been published elsewhere. For spectrally broad applications, a chirped QCD design was shown; it constitutes a first step towards semiconductor based ISB detectors. Together with an already demonstrated high speed capability and design flexibility, these features make QCDs to very interesting candidates for applications in various infrared wavelength ranges.

7. ACKNOWLEDGEMENTS

The authors acknowledge the generous financial support of the Swiss National Science Foundation. The project was made possible thanks to GEBERT-RÜF STIFTUNG in Basel, Switzerland, who provided start-up financing and project controlling. Technical assistance and valuable discussions with Marcel Graf, Milan Fischer, Marcella Giovannini, and Jérôme Faist are also gratefully acknowledged.

REFERENCES

1. B.F. Levine, K.K. Choi, C.G. Bethea, J. Walker, and R.J. Malik, "New 10 μm infrared detector using intersubband absorption in resonant tunneling GaAlAs superlattices" *Appl. Phys. Lett.* **50**, 1092 (1987)
2. H.C. Liu, J.M. Li, E.R. Brown, K.A. McIntosh, K.B. Nichols, and M.J. Manfra, "Quantum well intersubband heterodyne infrared detection up to 82 GHz" *Appl. Phys. Lett.* **67**, 1594 (1995)
3. H. Schneider and H.C. Liu, *Quantum well infrared photodetectors*. Springer (2006)
4. H.C. Liu, "Dependence of absorption-spectrum and responsivity on the upper state position in quantum-well intersubband photodetectors" *J. Appl. Phys.* **73**, 3062 (1993)

5. K.M.S.V. Bandara, J.W. Choe, M.H. Francombe, A.G.U. Perera, and Y.F. Lin, "GaAs/AlGaAs superlattice miniband detector with 14.5 μm peak response" *Appl. Phys. Lett.* **60**, 3022 (1992)
6. S.D. Gunapala, S.V. Bandara, J.K. Liu, C.J. Hill, S.B. Rafol, J.M. Mumolo, J.T. Trinh, M.Z. Tidrow, and P.D. LeVan, "Development of mid-wavelength and long-wavelength megapixel portable QWIP imaging cameras" *Infrared Physics & Technology* **47**, 67 (2005)
7. H. Schneider, P. Koidl, F. Fuchs, B. Dischler, K. Schwarz, and J.D. Ralston, "Photovoltaic intersubband detectors for 3-5 μm using GaAs quantum-wells sandwiched between AlAs tunnel barriers" *Semicond. Sci. Technol.* **6**, C120 (1991)
8. H. Schneider, K. Kheng, M. Ramsteiner, J.D. Ralston, F. Fuchs, and P. Koidl, "Transport asymmetry and photovoltaic response in (AlGa)As/AlAs/GaAs/(AlGa)As single-barrier quantum-well infrared detectors" *Appl. Phys. Lett.* **60**, 1471 (1992)
9. H. Schneider, "Optimized performance of quantum well intersubband infrared detectors: photovoltaic versus photoconductive operation" *J. Appl. Phys.* **74**, 4789 (1993)
10. M. Graf, G. Scalari, D. Hofstetter, J. Faist, H. Beere, E. Linfield, D. Ritchie, and G. Davies, "Terahertz range quantum well infrared photodetector" *Appl. Phys. Lett.* **84**, 475 (2004)
11. H.C. Liu, H. Luo, C. ying Song, Z. Wasilewski, A. SpringThorpe, and J. Cao, "Terahertz quantum well photodetectors" *IEEE Journal of Selected Topics in Quantum Electronics* **14**, 374 (2008)
12. L. Gendron, M. Carras, A. Huynh, V. Ortiz, C. Koeniguer, and V. Berger, "Quantum cascade photodetector" *Appl. Phys. Lett.* **85**, 2824 (2004)
13. M.A. Reed, US patents #4'878'104 (1987) and #5'165'065 (1992)
14. L. Gendron, C. Koeniguer, V. Berger, and X. Marcadet, "High resistance narrow band quantum cascade photodetectors" *Appl. Phys. Lett.* **86**, 121116 (2005)
15. M. Helm, *The basic physics of intersubband transitions*, *Semiconductors and semimetals* **62**, London, UK: Academic press (2000)
16. H.C. Liu, M. Buchanan, and Z. Wasilewski, "How good is the polarization selection rule for intersubband transitions?" *Appl. Phys. Lett.* **72**, 1682 (1998)
17. F.R. Giorgetta, E. Baumann, M. Graf, Q. Yang, C. Manz, K. Köhler, H.E. Beere, D.A. Ritchie, E Linfield, A.G. Davies, Y. Fedoryshyn, H. Jäckel, M. Fischer, J. Faist, and D. Hofstetter, "Quantum Cascade Detectors" *IEEE Journal of Quantum Electronics* **45**, 1029 (2009)
18. M. Graf, N. Hoyler, M. Giovannini, J. Faist, and D. Hofstetter, "InP-based quantum cascade detectors in the mid-infrared" *Appl. Phys. Lett.* **88**, 241118 (2006)
19. D.C. Larrabee, G.A. Khodaparast, J. Kono, K. Ueda, Y. Nakajima, M. Nakai, S. Sasa, M. Inoue, K.I. Kolokolov, J. Li, and C.Z. Ning, "Temperature dependence of intersubband transitions in InAs/AlSb quantum wells" *Appl. Phys. Lett.* **83**, 3936 (2003)
20. P. Cristea, Y. Fedoryshyn, J. F. Holzman, F. Robin, H. Jäckel, E. Müller, and J. Faist, "Tuning the intersubband absorption in strained AlAsSb/InGaAs quantum wells towards the telecommunications wavelength range" *J. Appl. Phys.* **100**, 116104 (2006)
21. F. R. Giorgetta, E. Baumann, D. Hofstetter, C. Manz, Q. Yang, K. Köhler, and M. Graf, "InGaAs/AlAsSb quantum cascade detectors operating in the near infrared" *Appl. Phys. Lett.* **91**, 111115 (2007)
22. D. Hofstetter, F.R. Giorgetta, E. Baumann, Q. Yang, C. Manz, and K. Köhler, "Mid-infrared quantum cascade detector with a spectrally broad response" *Appl. Phys. Lett.* **93**, 221106 (2008)